Journal of Computational Physics 229 (2010) 6696–6714

Contents lists available at ScienceDirect

Journal of Computational Physics

journal homepage: www.elsevier.com/locate/jcp

Absorbing boundary conditions for scalar waves in anisotropic media. Part 1: Time harmonic modeling

Siddharth Savadatti, Murthy N. Guddati *

Department of Civil, Construction and Environmental Engineering, North Carolina State University, Raleigh, NC 27695-7908, United States

ARTICLE INFO

Article history:
Received 19 March 2010
Received in revised form 19 May 2010
Accepted 20 May 2010
Available online 26 May 2010

Keywords:
Wave propagation
Perfectly matched layers
Group velocity
Rational approximation
Accuracy

ABSTRACT

With the ultimate goal of devising effective absorbing boundary conditions (ABCs) for general anisotropic media, we investigate the accuracy aspects of local ABCs designed for the scalar anisotropic wave equation in the frequency domain (time harmonic case). The ABC analyzed in this paper is the perfectly matched discrete layers (PMDL). PMDL is a simple variant of perfectly matched layers (PML) and is equivalent to rational approximation-based local ABCs. Specifically, we derive a sufficient condition for PMDL to accurately absorb wave modes with outgoing group velocities and this condition turns out to be a simple bound on the PMDL parameters. The reflection coefficient derived in this paper clearly reveals that the PMDL absorption is based on group velocities, and not phase velocities, and hence a PMDL can be designed to correctly identify and accurately absorb all outgoing wave modes (even those with opposing signs of phase and group velocities). The validity of the sufficient condition is demonstrated through a series of frequency domain simulations. In part 2 of this paper [S. Savadatti, M.N. Guddati, Absorbing boundary conditions for scalar waves in anisotropic media. Part 2: Time-dependent modeling, J. Comput. Phys. (2010), doi:10.1016/j.jcp.2010.05.017], the accuracy condition presented here is shown to govern both the well-posedness and accuracy aspects of PMDL designed for transient (time-dependent) modeling of scalar waves in anisotropic media.

1. Introduction

There exists a class of wave propagation problems defined on physically unbounded domains wherein the actual solution is required only in a small bounded region (the interior) which is separated from the rest of the unbounded domain (the exterior) by a computational boundary. Since the effect of the exterior is required only at the computational boundary, the computational domain can be restricted to just the interior by specifying *appropriate* absorbing boundary conditions (ABCs) that mimic the exterior by absorbing the outgoing waves at the computational boundary. In time harmonic modeling, appropriateness refers mainly to *accuracy* – the closeness of the computational model (interior + ABC) solution to the exact solution of the physical model (interior + exterior). In addition, computational *efficiency* is often critical for large scale simulations [1,2].

Exact ABCs are accurate by default, but their availability is restricted to simple exteriors with regular computational boundaries. They also tend to be prohibitively expensive for large scale simulations. Approximate ABCs that contain nonlocal spatial and temporal operators (global ABCs) are similarly unsuitable for large scale problems (in-spite of their accuracy) and hence local ABCs are preferred [1,2]. The most popular local ABCs currently available are rational ABCs and perfectly matched

* Corresponding author. Tel.: +1 919 515 7699; fax: +1 919 515 7908.
E-mail address: murthy.guddati@ncsu.edu (M.N. Guddati).

0021-9991/$ - see front matter © 2010 Elsevier Inc. All rights reserved.
doi:10.1016/j.jcp.2010.05.018

layers (PMLs) [3]. Rational ABCs approximate the exact stiffness (or associated dispersion relation) of an exterior with rational functions and were first introduced by Lindman [4]. Initial lower order implementations of Engquist and Majda's sequence of rational ABCs [5,6], Bayliss and Turkel's radiation BCs [7] and Higdon's multidirectional ABCs [8] were followed later by higher order formulations [9,10]. In one way or another, most of these formulations implemented higher order continued fraction expansions through the use of lower order functions of auxiliary variables and can be collectively called the auxiliary variable formulations. The other popular local ABC, the PML, is a 'special' absorbing medium that uses complex coordinate stretching to dampen out (or decay) propagating waves without creating artificial reflections at the computational boundary. The PML formulation was first introduced by Bérenger [11] and the complex coordinate stretching viewpoint was provided by Chew et al. [12–14]. Originally presented in a split variable formulation, PMLs are now available in unsplit forms along with variations like the conformal PML [15], complex frequency shifted PML (CFS-PML) [16], convolutional PML (CPML) [17] and multiaxial PML (M-PML) [18].

Currently, both rational ABCs and PMLs are available for a wide variety of governing equations that include, among many others, Maxwell's, linearized Euler's and elastodynamic equations. In comparison, neither ABC is absolutely superior to the other in all respects; the choice between the two is usually determined by specialized requirements of different problems. Rational ABCs tend to be more accurate than PML because the effect of the ABC parameters on solution accuracy is better understood in their case. On the other hand, ABCs based on PML have proven to be more versatile by being easily extendible to complicated exteriors [3]. The term complicated here implies material complications like heterogeneities and/or anisotropy and geometrical complications like corners and conformal boundaries.

In-spite of their many differences, rational ABCs and PML have deep underlying links as shown by Asvadurov et al. [19]. This link can be used to view certain rational ABCs as particular versions of PML e.g. a rational ABC designed purely for propagating waves can be viewed as an efficient form of PML with purely imaginary layer lengths. One such ABC is the perfectly matched *discrete* layer (PMDL), formerly known as continued fraction ABC (CFABC) [20,21]. PMDL uses mid-point integrated linear finite elements to approximate the stiffness of an unbounded domain *without* discretization error. The parameters of this approximation are the element lengths, which can in general be complex. The details of the PMDL formulation can be found in [22] and are summarized in Section 2.6. PMDL is known to possess several advantages over other local ABCs (see Section 2.6). Specifically, PMDL combines the accuracy of rational ABCs along with the versatility of PML and is thus used for the present study; moreover, the underlying links make the results of this paper applicable to other rational ABCs and PML in general.

In order to be accurate, ABCs should absorb most of the outgoing wave modes and, in the absence of exterior sources, they should not support incoming modes. While propagating waves are distinguished into incoming and outgoing wave modes depending on their group velocity, rational ABCs and PML have both been traditionally formulated to absorb waves depending on their phase velocities. This dependence on phase velocities (instead of group velocities) does not affect simple media where the phase and group velocities are always of the same sign (e.g. homogeneous isotropic acoustic medium) and hence accuracy requirements of ABC formulations for simple media have turned out to be relatively easy to satisfy. Recognizing the fact that many anisotropic and/or inhomogeneous media admit wave modes with opposing phase and group velocity directions, much recent research has been focused on developing techniques that result in accurate and stable ABCs for such media e.g. see [23–34] in reference to anisotropic or inhomogeneous (e.g. layered) electromagnetism, advective acoustics and elastodynamics. In particular reference to a medium governed by the linearized Euler equations, the inability of traditional PML to dampen outgoing wave modes in ducted domains in the presence of a mean flow was shown in [22] and attributed to the existence of wave modes with opposite signs of phase and group velocities. Space–time transformations proposed in [23,24] to address instabilities that were not at the time explicitly attributed to such modes, eventually became a remedy to this problem. Similar space–time transformations were developed in subsequent works [26–34] to specifically address the issue of opposing phase/group velocity signs in the case of acoustic, vorticity and entropy waves supported by the linearized Euler equations with parallel and oblique mean flows.

The scalar waves present in an anisotropic acoustic medium whose principal material axis is tilted with respect to the coordinate axis is one of the simple examples of a medium that allows wave modes with differing phase and group velocity signs (see Sections 2.3, 2.4). This paper provides a sufficient condition for accuracy of PMDL for time harmonic modeling of scalar waves in such an anisotropic medium. In essence, we prove that the parameters of PMDL (its layer lengths) need to satisfy a simple bound to be able to absorb outgoing wave modes without allowing incoming ones; this effectively guarantees accuracy. The criterion derived here, solely from the viewpoint of rational ABCs, bears similarity to the ones derived through coordinate transformations of PML and other ABCs in [26–34], even though the PMDL we use for this purpose *does not* require any coordinate transformation to be enforced. The absence of such transformations makes the PMDL ABC more amenable to extensions involving layered media.

This paper is concerned with the accuracy issues of the frequency domain analysis of the continuous problem with a straight computational boundary. Accuracy considerations here are limited to propagating waves only. As such, interior discretization errors, corners, curved computational boundaries and loss in accuracy due to neglecting the treatment of evanescent waves are outside the scope of this paper. It should be noted that the above restrictions are imposed to make the problem more tractable; they are, with the exception of curved boundaries, not due to any limitations of the PMDL formulation. PMDLs, capable of handling both propagating and evanescent waves for scalar isotropic media have already been implemented on domains with convex polygonal corners in [20]. As such, this paper can be considered as the necessary first

step towards a complete PMDL implementation for anisotropic media. An analogous study for the transient case can be found in Part 2 of this paper [36].

The outline of the rest of the paper is as follows. Section 2 contains preliminaries related to scalar anisotropic wave equation, followed by a discussion of the challenges inherent in designing accurate ABCs for such equations. A brief review of currently available ABCs is also presented in the same section followed by the choice of a particular ABC – the PMDL – that best suits the purposes of this paper. Section 3, which is the key to understanding the results of this paper, contains a detailed discussion of the approximation properties of PMDL along with a derivation of the reflection coefficient and a description of its interpolation points. A sufficient condition for accuracy of PMDL is derived in Section 4 by utilizing the reflection coefficient. Various numerical experiments are presented in Section 5 and finally, Section 6 contains a summary and conclusions.

2. Preliminaries

2.1. Model problem

The ultimate aim of this paper is to provide a practical ABC for the time-harmonic scalar anisotropic wave equation. To this end, we choose the simplest possible boundary in two dimensions: a straight edge without corners. Fig. 1 (*left*) shows such a boundary ($x = 0$) and the model problem shown therein consists of replacing the exact full-space by a left half-space (interior) along with an ABC that simulates the effect of the right half-space (exterior). The interior and exterior in Fig. 1 (*left*) are given by $x < 0$ and $x > 0$, respectively.

2.2. Scalar anisotropic media

We consider the time-harmonic scalar wave equation in two dimensions $(x - y)$ given by,

$$A\frac{\partial^2 u}{\partial x^2} + B\frac{\partial^2 u}{\partial y^2} + C\frac{\partial^2 u}{\partial x \partial y} + \omega^2 u = 0, \tag{1}$$

where the three independent parameters A, B, C define the material properties of the medium and ω is the temporal frequency. Eq. (1), e.g. arises in the study of anti-plane shear waves in transversely isotropic elastic media where the parameters A, B, C are functions of shear moduli, density and orientation of principal material axes of the medium. Similar scalar equations arise in the study of electromagnetism and advective acoustics.

For the sake of presentation, we Fourier transform (1) in y resulting in the reduced equation,

$$A\frac{\partial^2 u}{\partial x^2} - Bk_y^2 u + iCk_y\frac{\partial u}{\partial x} + \omega^2 u = 0, \tag{2}$$

where the following dualities apply:

$$\frac{\partial}{\partial y} \leftrightarrow ik_y \quad \text{and} \quad \frac{\partial}{\partial t} \leftrightarrow -i\omega. \tag{3}$$

For the sake of simplicity, the same notation u is used for both the field variable and its Fourier transform. In terms of individual modes, (1) admits solutions of the form $e^{ik_x x + ik_y y - i\omega t}$, where k_x and k_y are the horizontal and vertical wavenumbers, respectively. The horizontal wavenumber k_x is the root of the dispersion relation,

$$-Ak_x^2 - Bk_y^2 - Ck_x k_y + \omega^2 = 0. \tag{4}$$

In terms of horizontal slowness ($\sigma_x = k_x/\omega$) and vertical slowness ($\sigma_y = k_y/\omega$), (4) can be written as,

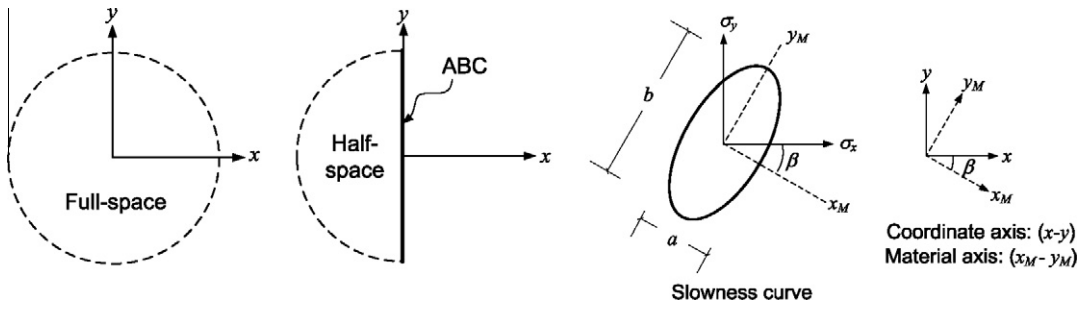

Fig. 1. *Left*: The model problem consists of replacing a full space by a left half-space and an efficient ABC that is accurate for a scalar anisotropic medium. *Right*: Global coordinate and material axes along with a typical slowness diagram for $(\sigma_x, \sigma_y) \in \mathbb{R}$. Note that the principal material axes (x_M, y_M) are shown on the ellipse just for reference.

$$-A\sigma_x^2 - B\sigma_y^2 - C\sigma_x\sigma_y + 1 = 0. \tag{5}$$

For $(\sigma_x, \sigma_y) \in \mathbb{R}$, (5) represents an ellipse in the slowness space that is completely defined by three independent parameters representing its semiminor axis (a), semimajor axis (b) and angle of tilt (β) with respect to the $x - y$ axis as shown in Fig. 1 (*right*). If we consider an anisotropic medium whose principal material axis (x_M, y_M) is tilted at an angle β with respect to the coordinate axes (x, y) (see Fig. 1), the wave equation in $x_M - y_M$ can be written as,

$$\frac{1}{a^2}\frac{\partial^2 u}{\partial x_M^2} + \frac{1}{b^2}\frac{\partial^2 u}{\partial y_M^2} + \omega^2 u = 0, \tag{6}$$

where the parameters a, b represent the material properties along x_M, y_M directions, respectively, e.g. if the medium has shear moduli μ_{x_M}, μ_{y_M} and density ρ, we have $1/a = \sqrt{\mu_{x_M}/\rho}$ and $1/b = \sqrt{\mu_{y_M}/\rho}$ (these are the wave velocities in $x_M - y_M$ directions). Eq. (1) is just the wave Eq. (6) expressed in $(x - y)$; simple coordinate rotations show that:

$$A = \left(\frac{\cos\beta}{a}\right)^2 + \left(\frac{\sin\beta}{b}\right)^2, \quad B = \left(\frac{\cos\beta}{b}\right)^2 + \left(\frac{\sin\beta}{a}\right)^2, \quad C = \sin 2\beta\left(\frac{1}{a^2} - \frac{1}{b^2}\right). \tag{7}$$

For later reference, we need the traction on the computational boundary ($x = 0$). For the medium defined by (6), the tractions in $x_M - y_M$ are $(a^{-2})\partial/\partial x_M$, $(b^{-2})\partial/\partial y_M$. These can be transformed into the tractions in $x - y$ through the usual second order tensor transformations to get,

$$T_x : A\frac{\partial u}{\partial x} + (C/2)\frac{\partial u}{\partial y}, \quad T_y : B\frac{\partial u}{\partial y} + (C/2)\frac{\partial u}{\partial x}, \tag{8}$$

where T_x, T_y are the tractions on surfaces perpendicular to x, y axes, respectively. Furthermore, without loss of generality, we consider the following with the direction of β being counter clockwise positive:

$$b \geqslant a > 0, \quad -\frac{\pi}{2} \leqslant \beta < \frac{\pi}{2}. \tag{9}$$

Eqs. (7) and (9) together ensure that

$$A > 0, \quad B > 0, \quad 4AB - C^2 > 0. \tag{10}$$

Variations of the three material properties A, B, C result in three kinds of slowness diagrams representing isotropic, untilted anisotropic and tilted anisotropic media as shown in Fig. 2. Since the solutions of (1) are of the form $e^{ik_x x + ik_y y - i\omega t}$, a wave mode can be defined as the solution for fixed k_y, ω, or equivalently, fixed σ_y. The behavior of such a mode in x direction is determined by the value of k_x which is the root of the dispersion relation (4).

2.3. Exact ABC

For a given mode i.e. for a fixed σ_y, (5) allows as its solutions, the two σ_x given by,

$$\sigma_x = \frac{-C\sigma_y \pm \sqrt{4A - (4AB - C^2)\sigma_y^2}}{2A} \tag{11}$$

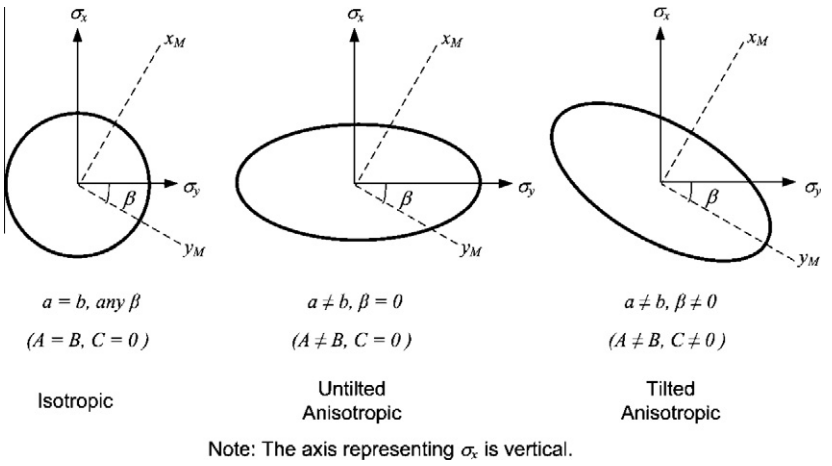

Fig. 2. Representative slowness diagrams for the three kinds of media governed by a scalar wave equation. Only slowness diagram for propagating waves is shown i.e. $(\sigma_x, \sigma_y) \in \mathbb{R}$. Note that the principal material axes (x_M,y_M) are shown on the ellipse just for reference.

Eq. (11) allows both propagating ($\sigma_x \in \mathbb{R}$) and evanescent modes ($\sigma_x \notin \mathbb{R}$). Each propagating wave mode is associated with a phase velocity (c_{px}) and a group velocity (c_{gx}) in the x-direction defined by:

$$\begin{aligned} c_{px} &= \frac{\omega}{k_x} = \frac{1}{\sigma_x}, \\ c_{gx} &= \frac{\partial \omega}{\partial k_x} = \frac{Ak_x + Ck_y/2}{\omega} = A\sigma_x + \frac{C\sigma_y}{2}. \end{aligned} \tag{12}$$

It is known that while c_{px} represents the apparent velocity of propagation, c_{gx} represents the true velocity of energy propagation in the x-direction. For the rest of the paper, the terms 'phase velocity' and 'group velocity' will refer to c_{px} and c_{gx}, respectively with the understanding that these velocities are always in the x direction. The propagating solutions of (11) can be classified in terms of c_{gx} as rightward and leftward propagating waves; their horizontal slownesses are given by,

$$\sigma_x = \frac{-C\sigma_y + \sqrt{4A - (4AB - C^2)\sigma_y^2}}{2A} : c_{gx} \geqslant 0 \ (\textit{rightward propagating}), \tag{13}$$

$$\sigma_x = \frac{-C\sigma_y - \sqrt{4A - (4AB - C^2)\sigma_y^2}}{2A} : c_{gx} \leqslant 0 \ (\textit{leftward propagating}). \tag{14}$$

Graphically, the propagating wave modes of (11) are represented by the ellipses in Fig. 3, where the rightward and leftward propagating waves of (13) and (14) are denoted by the solid and broken lines, respectively of the left ellipse in Fig. 3.

An exact right half-space, in the absence of any sources within it, admits waves that either propagate to the right ($c_{gx} \geqslant 0$) or decay with increasing x ($Im(\sigma_x) > 0$). The equation of an ABC that exactly simulates a right half-space is thus given by,

$$\sigma_x = \frac{-C\sigma_y + \sqrt{4A - (4AB - C^2)\sigma_y^2}}{2A} : \textit{Exact ABC (slowness form)}, \tag{15}$$

where the square root is defined by the standard branch cut and $(\sigma_y, \omega) \in \mathbb{R}$. The slowness diagram of an exact ABC for propagating waves ($\sigma_x \in \mathbb{R}$) will thus be the solid portion of the left ellipse in Fig. 3.

2.4. Approximate ABCs: need and challenges

It is known that, on inverse Fourier transforming, the square root in (15) results in pseudo differential operators that are global in both space and time [5]. An exact ABC is thus computationally expensive and hence ABCs that approximate (15), but lead to local operators are preferred.

Since the approximate ABC is supposed to represent the equation of an exact ABC (15) in some sense, it should try to capture, as accurately as possible, the solid part of the ellipse in Fig. 3 (left) i.e. the non-negative group velocity branch of the ellipse. An obvious sign of inaccuracy is the capturing of the negative group velocity branch. However, none of the approximate ABCs, neither rational ABCs nor PML, were developed with the explicit purpose of capturing positive group velocities. While the rational approximation of the square root operator employed by Engquist and Majda [5,6] ends up capturing the correct group velocities for scalar anisotropic waves, to the best of our knowledge it was never really implemented for the anisotropic case and hence it is not apparent that it would capture the right group velocities in general. Moreover, Engquist and Majda's ABCs are limited to scalar wave equations and robust extensions to vector systems may not be possible. A straightforward implementation of Higdon's multidirectional ABCs [8], as well as the complex coordinate stretching of PML in the direction of unboundedness can be shown to capture only positive phase velocities (*not* group velocities). This hardly poses a problem for the cases of isotropic or untilted anisotropic media (see Fig. 2) because

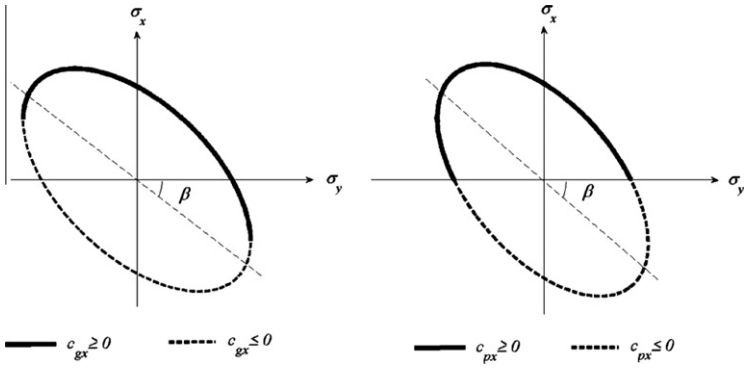

Fig. 3. A typical slowness diagram for tilted anisotropic media with the regions of positive group and phase velocities clearly demarcated.

every point on these slowness diagrams has phase and group velocities of the same sign. This can easily be inferred from (4), (7) and (12); because $C = 0$ for untilted anisoptropy and hence c_{gx} and c_{px} have the same sign. In fact, approximate ABCs that are well-posed, accurate and efficient for isotropic and untilted anisotropic media have existed for more than two decades, e.g. [5].

Consider however the case of tilted anisotropy. Fig. 3 clearly shows that there are portions on the slowness diagram which have group and phase velocities of differing signs. This implies that a typical approximate ABC (developed originally for isotropic or untilted anisotropic media and based on phase velocities) will try to capture the positive phase velocity branch (solid portion of the right ellipse in Fig. 3) instead of the positive group velocity branch (solid portion of the left ellipse in Fig. 3). Hence, such an approximate ABC is clearly inaccurate for tilted anisotropic media because it will end up capturing portions of the slowness diagram with negative group velocities. To demonstrate, frequency domain simulations transformed back in time are presented in Fig. 4. The figure on the left shows the wavefront in a tilted anisotropic acoustic medium of a source at the center of the domain. The wavefronts of the same source in domains half the size (dotted square) with ABCs applied at the truncated boundaries are shown in the two figures on the top and bottom right of Fig. 4. The two cases correspond to the same ABC with two different choices of the ABC parameters, *both* designed to capture positive *phase* velocities. The obvious inaccuracies due to reflections in the figure on the bottom right demonstrate the ineffectiveness of ABCs designed with reference to positive phase velocities.

2.5. Approximate ABCs: choices

As mentioned in the introduction, PML and rational ABCs are the most popular local ABCs; though seemingly disparate, recent works have demonstrated underlying links between the two. It was shown in [19] that optimal PML for propagating wave modes can be obtained by purely imaginary stretching and as such PML discretization is algebraically equivalent to rational ABCs obtained by approximating the square root operator. Hence, in the purely imaginary stretching case, rational ABCs can also be viewed as PML. The advantage of this viewpoint is that ABCs can now be developed to inherit the accuracy of rational ABCs while maintaining the versatility of PML. One such local ABC is the arbitrarily wide angle wave equation (AWWE) based CFABC first introduced in [37], with the underlying theory presented in [38] and linked to PML in [20]. These CFABCs can be viewed as particularly efficient discrete versions of PML where the '*perfect matching*' property of continuous PML is preserved even after discretization. This property of CFABCs later prompted the more appropriate term: 'Perfectly Matched *Discrete* Layers' (PMDLs) (see [22]).

PMDL forms the basis of this study because of their attractive properties (see [22,38]): (**a**) *Generality* – The PMDL formulation is applicable to general second order hyperbolic systems including (but not limited to) media governed by Maxwell's, linearized Euler's and elastodynamic equations, (**b**) *Completeness* – PMDL is capable of acting as an ABC for both propagating and evanescent waves, (**c**) *Accuracy* – *PMDL* can be implemented to an arbitrarily high degree of accuracy without a substantial loss in efficiency, (**d**) *Efficiency* – The PMDL formulation is local and is computationally efficient, (**e**) *Transparent* – The PMDL lends itself to explicit error calculation (the truncation error, the only kind of error in PMDL, can be calculated *a priori* for each wave mode), (**f**) *Versatility* – PMDL can be viewed as an optimal PML and hence it inherits the versatility of PML with respect to being extendible to complicated boundary geometries, and (**g**) *Ease of Use* – The PMDL formulation was derived within the finite element framework and can hence be directly incorporated into existing finite element or finite difference codes. Other ABCs that exhibit many of the above properties do exist. For example, although developed through a different, independent viewpoint, the auxiliary variable Hagstrom–Warburton formulation [39] can be shown to be equivalent to PMDL and exhibits most of the above properties. However, the derivation of Hagstrom–Warburton formulation is currently limited to the scalar case and as such it lacks the generality of PMDL.

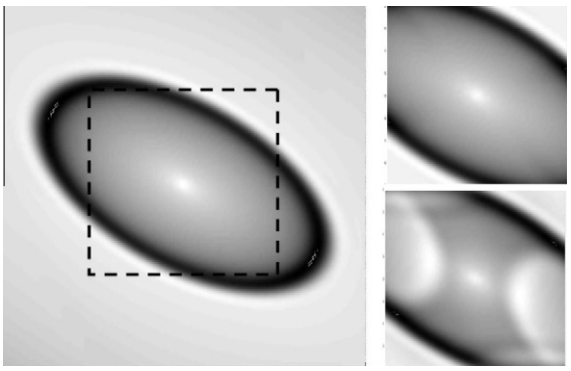

Fig. 4. *Left*: Wavefront in a tilted anisotropic acoustic medium of a source at the center of a domain. *Right*: Wavefronts of the same source in a truncated domain (dotted square) with ABCs designed to absorb positive *phase* velocities. The only difference in the two figures on the right is the choice of their ABC parameters.

Notwithstanding the above merits, effectiveness of PMDL is not assured, especially for general anisotropic and heterogeneous exteriors. The subsequent discussion is limited to propagating wave modes only, i.e. we are interested in properties of ABCs that only approximate the real part of (15). Even though neglecting evanescent modes ($\sigma_x \notin \mathbb{R}$) is expected to affect the long term accuracy of the solution in the interior [40], and even though PMDL *can* handle evanescent wave modes, we consider this paper to be a preliminary work on rational ABCs for tilted anisotropic media and so restrict ourselves to propagating wave modes.

2.6. PMDL formulation

PMDL derivation can best be presented in (x, σ_y, ω) space with the governing equation given by (2). Since we wish to replace the right half-space in Fig. 1 by an ABC, consider just the right half-space ($0 \leqslant x < \infty$) with a stiffness (or Dirichlet to Neumann map) given by K_{exact}. The traction F_0 on the left boundary ($x = 0$) and the field variable there (u_0), are related by:

$$F_0 = K_{exact} u_0 : \textit{Exact ABC } (\textit{stiffness form}). \tag{16}$$

Eq. (16) can be viewed as the stiffness form of the equation of an exact ABC as compared to the slowness form of (15). The traction for a tilted anisotropic medium governed by (2) is given by (8) and on the left boundary ($x = 0$), the traction T_x can be written as,

$$F_0 = -\left(A\frac{\partial}{\partial x} + \frac{C}{2} i\omega\sigma_y\right) u\Big|_{x=0}. \tag{17}$$

For a mode $u = e^{i\omega(\sigma_x x + \sigma_y y - t)}$, (16) with (17) leads to

$$K_{exact} = -i\omega\left(A\sigma_x + \frac{C}{2}\sigma_y\right). \tag{18}$$

In the absence of sources inside the right half-space, the horizontal slowness is given by (15). This allows us to write the exact stiffness (18) as

$$K_{exact} = \frac{-i\omega\sqrt{4A - (4AB - C^2)\sigma_y^2}}{2}. \tag{19}$$

PMDL approximates the exact stiffness K_{exact} in (19) by an approximate stiffness K_n to obtain an approximate ABC for Fig. 1 that mimics the absorption behavior of the right half-space; the PMDL equation approximating (16) takes the form,

$$F_0 = K_n u_0 : \textit{Approx ABC}(\textit{stiffness form}) \tag{20}$$

where the approximate stiffness K_n is obtained by using n mid-point integrated finite elements to approximate the stiffness of the right half-space at $x = 0$. The rationale behind this approximation can be summarized in the following four steps which are graphically depicted in Figs. 5 and 6.

[**STEP 1**] involves splitting the half-space $[0,\infty)$ into a finite element $[0,L_1]$ and another half-space $[L_1,\infty)$, with the finite element using linear shape functions to represent the displacement in $[0,L_1]$. As expected, the stiffness of the finite element $[0,L_1]$ plus half-space $[L_1,\infty)$ model can only approximate K_{exact} because of the error inherent in the finite element discretization.

[**STEP 2**] *which is the key to PMDL development*, involves the elimination of the finite element discretization error with respect to the half-space stiffness at $x = 0$. This is achieved by simply using mid-point integration to approximately eval-

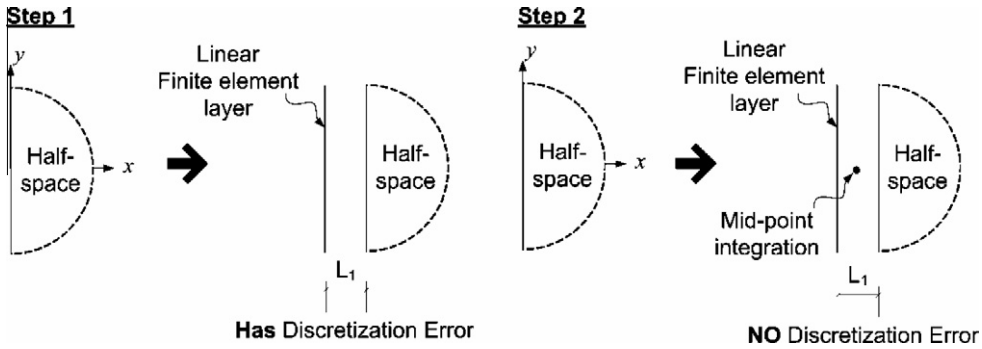

Fig. 5. Steps 1 and 2 of PMDL derivation: Replacing a half-space by a linear finite element and another half-space. The use of mid-point integration in the x direction eliminates the discretization error.

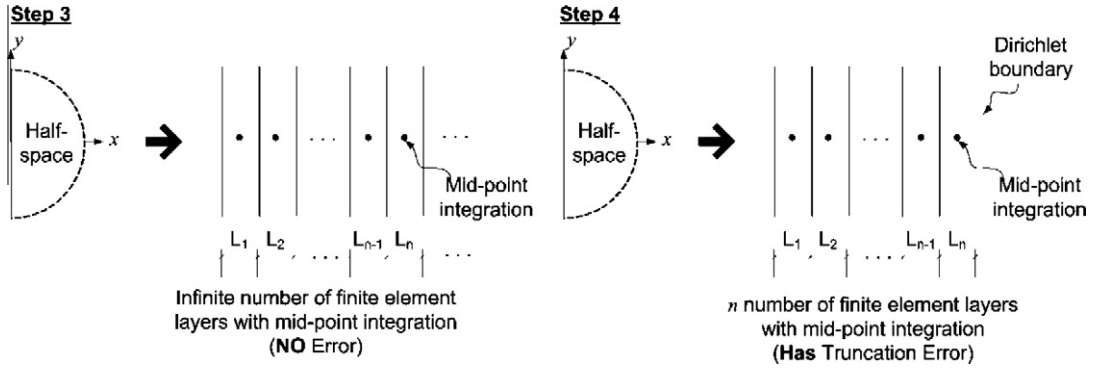

Fig. 6. Steps 3 and 4 of PMDL derivation: Replacing the half-space by an infinite number of mid-point integrated linear finite elements produces the exact stiffness at $x = 0$. Truncating the number of layers to n with a Dirichlet boundary at the end results in an implementable but approximate ABC; this is the n-layer PMDL.

uate the finite element stiffness matrix (see [20,21,38]). The stiffness of this mid-point integrated linear finite element is denoted by $\mathbf{S_j}$ (with $j = 1$) with $\sigma_{x1} = 2i/\omega L_1$:

$$\mathbf{S_j} = \begin{bmatrix} S_j^{11} & S_j^{12} \\ S_j^{21} & S_j^{22} \end{bmatrix} = \frac{-i\omega\sigma_{xj}A}{2}\begin{bmatrix} 1 & -1 \\ -1 & 1 \end{bmatrix} + \frac{iC\omega\sigma_y}{2}\begin{bmatrix} 0 & -1 \\ 1 & 0 \end{bmatrix} + \frac{i\omega\left(B\sigma_y^2 - 1\right)}{2\sigma_{xj}}\begin{bmatrix} 1 & 1 \\ 1 & 1 \end{bmatrix} \quad \text{for}(j = 1 \ldots n) \tag{21}$$

Note that the mid-point integrated linear finite element $[0, L_1]$ plus half-space $[L_1, \infty)$ model represents the *exact* stiffness of the original half-space $[0, \infty)$ at $x = 0$ *irrespective* of the element length L_j; it can be arbitrarily large and is not even restricted to real numbers.

[**STEP 3**] involves applying the above splitting recursively to discretize the original half-space into an infinite number of finite element layers, $[0, L_1]$, $[L_1, L_1 + L_2]$, ... as shown in Fig. 6. Such splitting does not introduce any further discretization error because the mid-point integration in step 2 eliminates *all* discretization errors in the half-space stiffness. Hence, this discretized half-space containing an infinite number of layers is *exact* as far as the stiffness at $x = 0$ (K_{exact}) is concerned.

[**STEP 4**] involves limiting the number of layers for computational tractability. The number of layers is limited to n with a Dirichlet boundary condition $u_n = 0$ applied at $x = \sum L_j$ as shown in Fig. 6. This results in a n-layer finite element model of the half-space whose stiffness K_n can be written in the continued fraction form:

$$K_n = S_1^{11} - \cfrac{S_1^{12}S_1^{21}}{S_1^{22} + S_2^{11} - \cfrac{S_2^{12}S_2^{21}}{S_2^{22} + S_3^{11} - \cfrac{}{\ddots \; \cfrac{S_{n-1}^{12}S_{n-1}^{21}}{S_{n-1}^{22} + S_n^{11}}}}}. \tag{22}$$

The above expression is obtained by assembling the n element matrices $\mathbf{S_j}$ ($j = 1 \ldots n$) in (21) and eliminating the auxiliary variables $u_1, \ldots u_{n-1}$. Note that the truncation to n layers introduces errors, which makes K_n an approximation of K_{exact}. Hence (20) is the equation of an approximate ABC which will be referred to as the n-layer PMDL.

In (21), σ_{xj} with ($j = 1 \ldots n$) are termed the n parameters of PMDL. The finite element layer lengths L_j are related to these parameters as $L_j = 2i/\omega\sigma_{xj}$. This particular choice of frequency dependent imaginary lengths ensures that the boundary condition, when transformed back into the time domain, will have all real-valued coefficients, thus avoiding any complex arithmetic [38]. Comparing (20) to (16) we see that PMDL approximates the exact stiffness ($K_n \approx K_{exact}$) and the properties of this approximation are dictated solely by the choice of the n arbitrary parameters σ_{xj}. A detailed derivation of the formulation presented in this subsection is given in [38]. For later use, the following identities can be easily derived from (19) and (21):

$$\begin{aligned} S_j^{11} &= S_j^{22}, \\ K_{exact}^2 &= S_j^{11}S_j^{22} - S_j^{12}S_j^{21}. \end{aligned} \tag{23}$$

2.7. Objective

To restate, the objective of this paper is to develop an accurate PMDL for scalar wave propagation in tilted anisotropic media. Specifically, we will derive criteria for the parameters σ_{xj} that will make the n-layer PMDL an accurate ABC for the model problem in Fig. 1.

3. PMDL: Approximation properties

In this section, we closely examine the approximation properties of PMDL for tilted anisotropic media. This section is key to understanding the rest of the paper.

3.1. General approximation properties

The PMDL presented in the previous section is a special form of rational ABCs. Rational ABCs use rational functions $P_{r,s}$ of the form,

$$P_{r,s}(\sigma_y) = \frac{p_r(\sigma_y)}{q_s(\sigma_y)}, \tag{24}$$

to approximate the irrational square root operator present in the definition of an exact ABC (15). Here p_r and q_s are polynomials of exact degrees $r \geqslant 0$ and $s \geqslant 0$, respectively with no common zeros. In the case of isotropic and untilted anisotropic media, for a particular choice of r,s and the $r+s+2$ coefficients of p_r and q_s, the dispersion relation of every rational ABC can be represented as $\sigma_x = P_{r,s}(\sigma_y)$. This dispersion relation can be viewed as an approximation of the dispersion relation of the exact ABC (15). Using $C=0$ in (15), we get the exact ABC for isotropic and untilted anisotropic media as $\sigma_x = +\sqrt{A(1-B\sigma_y^2)}/A$. Hence, rational ABCs for isotropic and untilted anisotropic media approximate the irrational square root by a rational function i.e. $P_{r,s}(\sigma_y) \approx +\sqrt{A(1-B\sigma_y^2)}/A$.

PMDL approximates the exact stiffness K_{exact} in (16) by K_n. The continued fraction form of K_n in (22) can also be expressed as

$$K_n = -i\omega P_{2n,2n-2}(\sigma_y). \tag{25}$$

Using $K_n \approx K_{exact}$, (19) and (25) we can see that the n-layer PMDL is equivalent to a rational approximation of the positive square root operator,

$$P_{2n,2n-2}(\sigma_y) \approx \frac{+\sqrt{4A-(4AB-C^2)\sigma_y^2}}{2}. \tag{26}$$

The rational approximation of (26) can be used in the slowness form of the exact ABC in (15) to obtain the slowness form of the n-layer PMDL as

$$\sigma_x = \frac{-C\sigma_y/2 + P_{2n,2n-2}(\sigma_y)}{A} \quad : \textit{Approx ABC(slowness form)}. \tag{27}$$

As far as this paper is concerned, we are interested in modeling propagating waves only. When the parameters of n-layer PMDL σ_{xj} are chosen to be real, $P_{2n,2n-2}$ becomes a real rational function and (27) approximates the real part of (15) i.e. (27) treats propagating waves only. Hence we restrict ourselves to $\sigma_{xj} \in \mathbb{R}$. A few points need to be clarified here. (a) It should be noted that a choice of $\sigma_{xj} \in \mathbb{R}$ is in no way due to a limitation of the PMDL itself. It has already been shown that PMDL models propagating waves for purely real σ_{xj}, evanescent waves for purely imaginary σ_{xj} and both propagating and evanescent waves for complex σ_{xj} [38]. (b) Choosing purely real σ_{xj} also implies choosing purely imaginary finite element layer lengths since we assumed $L_j = 2i/\omega\sigma_{xj}$. This should not pose any problem because, as mentioned in Step 2 of Section 2.6, the elimination of discretization error due to mid-point integration is independent of L_j. (c) Since L_j can be real, imaginary or complex, the domain $x \in (0, \sum L_j)$ of the n-layer PMDL can, in general, be complex; this complex domain in no way represents *or* approximates the physical right half-space that forms the exterior $[0,\infty)$. However, the stiffness of this n-layer PMDL at $x=0$ is an approximation of the stiffness of the right half-space i.e. $K_n \approx K_{exact}$.

3.2. Reflection coefficient

The reflection coefficient is defined as the ratio of amplitudes of the reflected wave to the incident wave and the approximation properties of an ABC designed for propagating waves can be studied through the magnitude of its reflection coefficient. The reflection coefficient R_n for a n-layer PMDL can be derived by considering individual propagating wave modes with a fixed $(\sigma_y, \omega) \in \mathbb{R}$. Since we are interested in propagating wave modes only, σ_y is chosen so as to yield real σ_x. The dispersion relation (5) admits two σ_x for a given σ_y. These two modes (13) and (14) have group velocities that are negative of each other and can be categorized into rightward and leftward propagating waves. For the left half-space with an approximate ABC at $x=0$, we can consider the rightward propagating wave as the incident wave on the boundary $x=0$ and the leftward propagating wave as the reflected wave. Using the definition of reflection coefficient, the total wave field in the left half-space can be represented by $u = e^{i\omega(\sigma_x x+\sigma_y y-t)} + R_n e^{i\omega(\tilde{\sigma}_x x+\sigma_y y-t)}$ where σ_x and $\tilde{\sigma}_x$ are the two roots given by (13) and (14), respectively. Since σ_x is the slowness in the incident wave mode $e^{i\omega(\sigma_x x+\sigma_y y-t)}$, it is the root with the non-negative group velocity i.e. $c_{gx} = +\sqrt{4A-(4AB-C^2)\sigma_y^2}/2 \geqslant 0$. The other root can be written as $\tilde{\sigma}_x = -(\sigma_x + C\sigma_y/A)$ and the reflected wave mode $e^{i\omega(\tilde{\sigma}_x x+\sigma_y y-t)}$ has non-positive group velocity. The reflection coefficient derivation will not need a precise classification of zero

group velocity modes as either incident or reflected modes; hence the obvious overlap between rightward and leftward propagating modes for $c_{gx} = 0$ can be neglected. Substituting u into the equation defining a n-layer PMDL (20) and using (17), we get:

$$\omega\left(-iA(\sigma_x + R_n\tilde{\sigma}_x) - i\frac{C}{2}(1+R_n)\sigma_y\right)e^{i\omega(\sigma_y y - t)} = K_n u_0. \tag{28}$$

Since the displacement $u_0 = u|_{x=0} = (1+R_n)e^{i\omega(\sigma_y y - t)}$, (28) becomes,

$$(1+R_n)K_n = -i\omega A(\sigma_x + R_n\tilde{\sigma}_x) - i\omega\frac{C}{2}(1+R_n)\sigma_y. \tag{29}$$

We can solve for the reflection coefficient R_n in (29) and write it either in terms of slowness or stiffness. Using $\tilde{\sigma}_x = -(\sigma_x + C\sigma_y/A)$, (13) and (25), (29) can be written in slowness form as,

$$R_n = \left(\frac{\sqrt{4A - (4AB - C^2)\sigma_y^2}/2 - P_{2n,2n-2}(\sigma_y)}{\sqrt{4A - (4AB - C^2)\sigma_y^2}/2 + P_{2n,2n-2}(\sigma_y)}\right) : \textit{Reflection coefficient}(\textit{slowness form}). \tag{30}$$

On the other hand, using $\tilde{\sigma}_x = -(\sigma_x + C\sigma_y/A)$ and (18), (29) can be written in stiffness form as,

$$R_n = \left(\frac{K_{exact} - K_n}{K_{exact} + K_n}\right) : \textit{Reflection coefficient}(\textit{stiffness form}). \tag{31}$$

Expressions (30) and (31) are of course equivalent to each other considering (19) and (25). From (22) and (23) we have $K_n = K_{exact}^2/\left(S_n^{11} + K_{n-1}\right)$. This allows us to write (31) in the recursive form,

$$R_n = \left(\frac{S_n^{11} - K_{exact}}{S_n^{11} + K_{exact}}\right)R_{n-1}. \tag{32}$$

Since the reflection coefficient for the 0-layer PMDL (the Dirichlet boundary in Fig. 6) is $R_0 = -1$, the magnitude of the reflection coefficient turns out to be (in stiffness form),

$$|R_n| = \left|\prod_{j=1}^{n}\left(\frac{S_j^{11} - K_{exact}}{S_j^{11} + K_{exact}}\right)\right|. \tag{33}$$

By utilizing (18), (19) and (23), the reflection coefficient of (33) can be also written in slowness form as:

$$|R_n| = \left|\prod_{j=1}^{n}\left(\frac{A\sigma_x - A\sigma_{xj}}{A\sigma_x + A\sigma_{xj}}\right)\left(\frac{A(\sigma_x - \sigma_{xj}) + C\sigma_y}{A(\sigma_x + \sigma_{xj}) + C\sigma_y}\right)\right|. \tag{34}$$

An exact ABC produces no reflections and hence its reflection coefficient is zero for all wave modes ($R \equiv 0$). The n-layer PMDL results in $R_n = 0$ for only some (not all) modes and these are termed the reference modes. The horizontal slownesses of the reference modes are termed the reference slownesses. By setting $R_n = 0$ in (34), the reference slownesses can be seen to be

$$\sigma_x = \sigma_{xj}, \sigma_{xj} - (C/A)\sigma_y. \tag{35}$$

The choice of the notation σ_{xj} for the parameters of the PMDL is now apparent because they represent some of the horizontal slownesses for which the PMDL is exact. The form of the reflection coefficient in (34) can be specialized for isotropic media by substituting $C = 0$ and compared to the reflection coefficient derived in [21] for isotropic acoustics.

Since we are interested in the ability of PMDL to absorb wave modes with non-negative group velocities, we rearrange (34) to get

$$|R_n| = \left|\prod_{j=1}^{n}\left(\frac{A\sigma_x - A\sigma_{xj}}{A(\sigma_x + \sigma_{xj}) + C\sigma_y}\right)\left(\frac{A(\sigma_x - \sigma_{xj}) + C\sigma_y}{A\sigma_x + A\sigma_{xj}}\right)\right| = \left|\prod_{j=1}^{n}\left(\frac{c_{gx} - (A\sigma_{xj} + (C/2)\sigma_y)}{c_{gx} + (A\sigma_{xj} + (C/2)\sigma_y)}\right)\left(\frac{c_{gx} - (A\sigma_{xj} - (C/2)\sigma_y)}{c_{gx} + (A\sigma_{xj} - (C/2)\sigma_y)}\right)\right|. \tag{36}$$

From (12), (18) and (19) we have $c_{gx} = A\sigma_x + (C/2)\sigma_y = +\sqrt{4A - (4AB - C^2)\sigma_y^2}/2 \geqslant 0$. Hence the group velocity in (36) is non-negative, i.e. it is the group velocity of the incident wave mode propagating rightward ($c_{gx} \geqslant 0$).

Eq. (36) shows that for a given $\sigma_y \in \mathbb{R}$, $R_n = 0$ for all modes with group velocities $c_{gx} = A\sigma_{xj} + (C/2)\sigma_y$ and $c_{gx} = A\sigma_{xj} - (C/2)\sigma_y$. Hence these are referred to as the reference group velocities corresponding to the reference slownesses in (35). Noting that the PMDL is exact for the reference modes, the reference slownesses (35) should satisfy the exact dispersion relation (5). Substituting (35) separately in (5), we get the following reference group velocities:

$$A\sigma_{xj} + (C/2)\sigma_y = A\sigma_{xj} + (C/2)\left(\frac{-C\sigma_{xj} \pm \sqrt{4B - (4AB - C^2)\sigma_{xj}^2}}{2B}\right),$$
$$A\sigma_{xj} - (C/2)\sigma_y = A\sigma_{xj} - (C/2)\left(\frac{C\sigma_{xj} \pm \sqrt{4B - (4AB - C^2)\sigma_{xj}^2}}{2B}\right). \tag{37}$$

Note that either the positive or the negative square root should be chosen in both the equations of (37) and either choice leads to the same pair of group velocities. By defining,

$$c_j = A\sigma_{xj} + (C/2)\left(\frac{-C\sigma_{xj} + \sqrt{4B - (4AB - C^2)\sigma_{xj}^2}}{2B}\right),$$
$$\bar{c}_j = A\sigma_{xj} + (C/2)\left(\frac{-C\sigma_{xj} - \sqrt{4B - (4AB - C^2)\sigma_{xj}^2}}{2B}\right), \tag{38}$$

we can rewrite (36) using (37) and (38) as:

$$|R_n| = \left|\prod_{j=1}^{n}\left(\frac{c_{gx} - c_j}{c_{gx} + c_j}\right)\left(\frac{c_{gx} - \bar{c}_j}{c_{gx} + \bar{c}_j}\right)\right| (c_{gx} \geqslant 0) : \textit{Reflection coefficient}(\textit{group velocity form}). \tag{39}$$

For any given parameter σ_{xj}, the PMDL is exact ($R_n = 0$) for wave modes with two different group velocities c_j, $\bar{c}_j$ given by (38) and hence these are the reference group velocities. The requirement $c_{gx} \geqslant 0$ in (39) is just a reminder that the c_{gx} in (39) is the group velocity of the incident wave mode that is propagating rightward.

3.3. Points of interpolation

Since the n-layer PMDL is exact for the reference modes, the vertical and horizontal slowness pairs of these modes are the points at which (27) interpolates (11). The reference horizontal slownesses given by (35) can be substituted in (11) to get the reference vertical slownesses $\sigma_y = \pm\sigma_{yj}, \pm\bar{\sigma}_{yj}$, where,

$$\sigma_{yj} = \frac{-C\sigma_{xj} + \sqrt{4B - (4AB - C^2)\sigma_{xj}^2}}{2B},$$
$$\bar{\sigma}_{yj} = \frac{-C\sigma_{xj} - \sqrt{4B - (4AB - C^2)\sigma_{xj}^2}}{2B}. \tag{40}$$

For a given parameter σ_{xj}, there exist two reference group velocities (c_j, $\bar{c}_j$), and for each reference group velocity, there exist two reference wave modes. Hence there are four reference modes for every σ_{xj}; these four modes (with their group velocities) are given by:

$$\left.\begin{array}{l} e^{i\omega(\sigma_{xj}x + \sigma_{yj}y - t)} \\ e^{i\omega((\sigma_{xj} + (C/A)\sigma_{yj})x - \sigma_{yj}y - t)} \end{array}\right\} \quad c_{gx} = c_j,$$
$$\left.\begin{array}{l} e^{i\omega(\sigma_{xj}x + \bar{\sigma}_{yj}y - t)} \\ e^{i\omega((\sigma_{xj} + (C/A)\bar{\sigma}_{yj})x - \bar{\sigma}_{yj}y - t)} \end{array}\right\} \quad c_{gx} = \bar{c}_j. \tag{41}$$

Hence, for every σ_{xj}, the PMDL slowness (27) interpolates the exact slowness (11) at the four points given by $(\sigma_{yj}, \sigma_{xj})$, $(-\sigma_{yj}, \sigma_{xj} + (C/A)\sigma_{yj})$, $(\bar{\sigma}_{yj}, \sigma_{xj})$ and $(-\bar{\sigma}_{yj}, \sigma_{xj} + (C/A)\bar{\sigma}_{yj})$. It should be noted that these four points of interpolation need not necessarily be distinct; For $C \neq 0$ (tilted anisotropy of Fig. 2), there are indeed four distinct points of interpolation when $\sigma_{xj} \neq \pm\sqrt{4B/(4AB - C^2)}$ but only two distinct points of interpolation (each with multiplicity 2) when $\sigma_{xj} = \pm\sqrt{4B/(4AB - C^2)}$. Similarly for $C = 0$ (isotropy and untilted anisotropy of Fig. 2), there are two distinct points of interpolation (each with multiplicity 2) when $\sigma_{xj} \neq \pm\sqrt{4B/(4AB - C^2)}$ and just one point of interpolation (with a multiplicity of 4) when $\sigma_{xj} = \pm\sqrt{4B/(4AB - C^2)}$. However, for every choice of σ_{xj}, there are four points of interpolation counted *with multiplicity*. Since a n-layer PMDL has n parameters (σ_{xj} with $j = 1 \ldots n$), it has $4n$ points of interpolation in all counted with multiplicity. These $4n$ points for a single layer PMDL ($n = 1$) are graphically represented on a typical slowness curve in Fig. 7 (left).

A few observations about interpolation points should be kept in mind: (a) A choice of real parameters $\sigma_{xj} \in \mathbb{R}$ may lead to complex σ_{yj} and $\bar{\sigma}_{yj}$. This means that the interpolation points need not be real and hence may not be depicted on a typical slowness diagram which is a plot of $(\sigma_y, \sigma_x) \in \mathbb{R}$. However, (27) still interpolates (11), albeit now in complex space

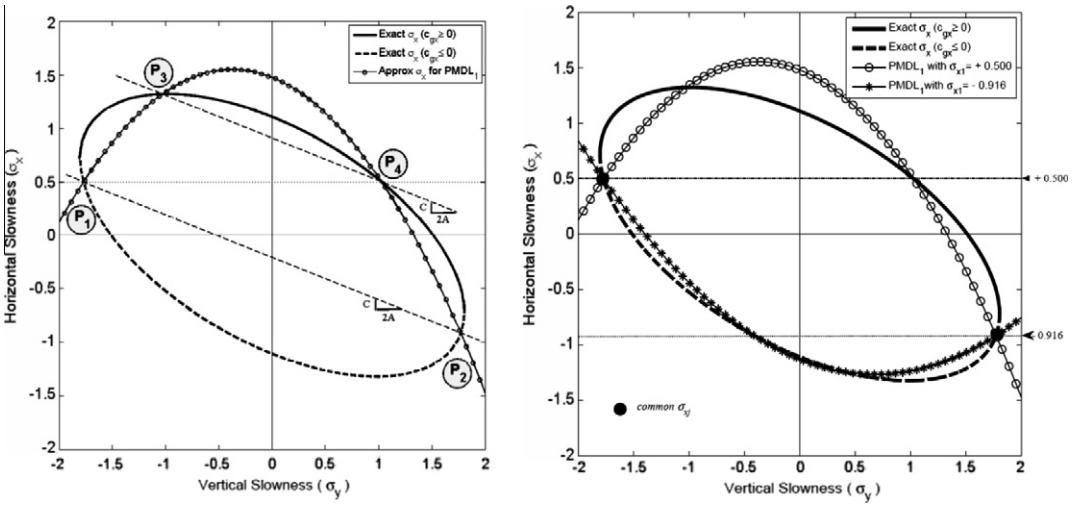

Fig. 7. *Left*: The four points of at which a 1 layer PMDL dispersion relation (approximate) matches the exact dispersion relation are the four modes for which the 1 layer PMDL is exact. *Right*: The two parameters σ_{xj} that result in a particular reference group velocity of c_j (or $\bar{c}_j$) for a 1 layer PMDL.

$(\sigma_y, \sigma_x) \in \mathbb{C}$. (b) We can choose the parameters σ_{xj} arbitrarily but we cannot choose the two related reference group velocities $(c_j, \bar{c}_j)$ independent of one another. Of the three – σ_{xj}, c_j, $\bar{c}_j$ – only one can be chosen. A choice of σ_{xj} uniquely determines c_j and $\bar{c}_j$ from (38) and this is the only choice that we truly have. For theoretical purposes however, it may appear advantageous to be able to design a PMDL that is exact for a given group velocity. This is equivalent to choosing c_j (or $\bar{c}_j$). A choice of c_j (or $\bar{c}_j$) however can be obtained from two different σ_{xj} in general and this in turn results in two different $\bar{c}_j$ (or c_j) – this is shown in Fig. 7. Because of this ambiguity, we focus on σ_{xj} as the parameters of the PMDL. Note that this is true only for tilted anisotropy; in the untilted anisotropic or isotropic case, there is a unique parameter for a given group velocity.

4. Accuracy

4.1. Accuracy criterion

The ideal accuracy criterion for a n-layer PMDL is $R_n(c_{gx}) = 0$ for all $c_{gx} \geqslant 0$. We use $R_n(c_{gx})$ to emphasize the fact that the reflection coefficient is a function of the group velocity of the incident wave mode (see (39)). The reflection coefficient of a n-layer PMDL (39) is zero for exactly $2n$ group velocities given by the reference group velocities c_j, $\bar{c}_j$ ($j = 1 \ldots n$). Hence, the ideal of $R_n(c_{gx}) = 0$ for all $c_{gx} \geqslant 0$ can never be realized in practice by a n-layer PMDL with a finite n. This necessitates the formulation of an attainable accuracy criterion.

Accuracy criterion: An n-layer PMDL is considered accurate if, by increasing the number of layers n, the magnitude of its reflection coefficient can be made arbitrarily small for every rightward propagating wave mode, i.e.

$$\lim_{n\to\infty} |R_n(c_{gx})| = 0 \quad \forall\ c_{gx} \geqslant 0 : \textit{Accuracy criterion}. \tag{42}$$

To be precise (42) is a *convergence* criterion that is necessary for a PMDL to act as a meaningful ABC for rightward propagating waves. If the rate of convergence is slow, the number of PMDL layers required for sufficient accuracy might render the ABC inefficient. The usage of the term *accuracy* instead of the term *convergence* is mainly for the sake of compatibility with existing ABC literature.

4.2. Sufficient condition for accuracy

In order to facilitate the derivation of conditions under which a PMDL is accurate, we restate the accuracy criterion and reformulate the reflection coefficient. The accuracy criterion (42), written separately for zero and positive group velocities is:

$$\lim_{n\to\infty} |R_n(c_{gx})| = 0 \quad \text{for} \quad c_{gx} = 0, \tag{43}$$

$$\lim_{n\to\infty} |R_n(c_{gx})| = 0 \quad \forall\ c_{gx} > 0. \tag{44}$$

The reflection coefficient is given by (39) and can be expressed as:

$$|R_n| = \left|\prod_{j=1}^{n} R_{nj}\right| = \left|\prod_{j=1}^{n} r_j \bar{r}_j\right|, \tag{45}$$

where,

$$R_{nj} = r_j \bar{r}_j, \quad r_j = \left(\frac{c_{gx} - c_j}{c_{gx} + c_j}\right), \quad \bar{r}_j = \left(\frac{c_{gx} - \bar{c}_j}{c_{gx} + \bar{c}_j}\right) \quad \text{for } c_{gx} \geqslant 0, j = 1 \ldots n. \tag{46}$$

The accuracy criteria (43) and (44) can be satisfied by choosing either zero, negative or positive reference group velocities $(c_j, \bar{c}_j)$ in (45) and (46).

Consider (43) with various (zero, negative and positive) reference group velocities. Criterion (43) cannot be satisfied if all reference group velocities are non-zero because in this case, $|R_n| = 1$ and hence $\lim_{n\to\infty}|R_n| = 1$ for $c_{gx} = 0$. One way to ensure accuracy for $c_{gx} = 0$ is to have at least one zero reference group velocity. This makes the n-layer PMDL exact for zero group velocity modes and hence by definition $|R_n| = 0$ for $c_{gx} = 0$ (which satisfies (43)). In other words, the PMDL will allow wave modes with $c_{gx} = 0$ to exist in the left half-space (interior). While this is perfectly acceptable from the viewpoint of accuracy – an exact right half-space that the PMDL is trying to emulate does allow zero group velocity modes in the interior – we do not allow zero reference group velocity because of the following reasons. Since untilted anisotropy (and isotropy) are special cases of tilted anisotropy, we expect the conclusions presented here to hold for these cases as well i.e. for the case $C = 0$ in Fig. 2. But from (38), it is clear that for $C = 0$, a zero reference group velocity translates to $\sigma_{xj} = 0$ which in turn requires $L_j = \infty$. This is not practically feasible and we violate (43) and consider the PMDL with $|R_n| = 1$ (and with $\lim_{n\to\infty}|R_n| = 1$) for $c_{gx} = 0$ to be *'accurate enough'*. An even more potent reason for not allowing zero reference group velocites is that such a choice will lead to ill-posedness of the ABC in *transient* modeling of acoustic waves (see [41]). Moreover, for the case of untilted anisotropy and isotropy, (43) cannot be satisfied by any local ABC. This discussion thus eliminates (43) and entirely excludes the choice of zero reference group velocities. This leaves us with a choice of positive or negative reference group velocities in trying to satisfy (44).

Consider the choice of negative reference group velocities in ensuring (44). Without loss of generality let $c_1 < 0$. As $c_{gx} \to -c_1(>0)$, we have $|r_1| \to \infty$. Unless there is another factor r_j or $\bar{r}_j$ in (45) that tends to zero as fast or faster than $|r_1| \to \infty$, the reflection coefficient will grow without bound ($|R_n| \to \infty$) and hence (44) cannot be satisfied for c_{gx} in the neighborhood of $-c_1$. It is however possible to prevent the unbounded growth in $|R_n|$ by a careful choice of other reference group velocities. For example if $c_2 = -c_1$, then $|r_2| \to 0$ as $c_{gx} \to -c_1$. The reflection coefficient need not necessarily tend to ∞ now because $|r_1 r_2| = 1$ and this prevents the unbounded growth of $|R_n|$ due to $|r_1| \to \infty$. However, such a choice of parameters results in a loss of factors in the expression for R_n; the factor r_2 is 'lost' in canceling out the effect of r_1 and does not contribute to reducing the reflection coefficient. In many cases this reduces the efficiency of a PMDL i.e. we might need a larger n to ensure a sufficiently small R_n. Hence, we will not consider negative reference group velocities unless they are necessary for meeting the accuracy criterion (44).

Fortunately, it is possible to satisfy (44) with only positive reference group velocities. Noting the product form of (45), the accuracy criterion (44) is satisfied if each term in the product is less than one. Thus, a sufficient condition for (44) is:

$$|R_{nj}| < 1 \quad \forall\ c_{gx} > 0. \tag{47}$$

It is obvious from (45) that a choice of positive reference group velocities ($c_j > 0$ and $\bar{c}_j > 0$) is sufficient for (47) to be satisfied. Hence a choice of $c_j > 0$ and $\bar{c}_j > 0$ is also sufficient for (44). Using (38), this sufficient condition becomes

$$A\sigma_{xj} + (C/2)\left(\frac{-C\sigma_{xj} \pm \sqrt{4B - (4AB - C^2)\sigma_{xj}^2}}{2B}\right) > 0. \tag{48}$$

Using (10), (48) can be reduced to,

$$(4AB - C^2)\sigma_{xj} > \left|C\sqrt{4B - (4AB - C^2)\sigma_{xj}^2}\right|. \tag{49}$$

Noting that $4AB - C^2 > 0$ (see (10)), (49) can be reduced to,

$$\sigma_{xj} > \frac{\left|C\sqrt{4B - (4AB - C^2)\sigma_{xj}^2}\right|}{(4AB - C^2)}, \tag{50}$$

which, on squaring and rearranging results in,

$$\sigma_{xj} > \left|\frac{C}{\sqrt{A(4AB - C^2)}}\right|. \tag{51}$$

The condition (51) has a simple geometric interpretation that is shown in Fig. 8 (left).

The above discussion (from (48) onward) implicitly assumed that $c_j, \bar{c}_j \in \mathbb{R}$ which is not true when $\sigma_{xj} > 2\sqrt{B}/(\sqrt{4AB - C^2})$. However, for $\sigma_{xj} > 2\sqrt{B}/(\sqrt{4AB - C^2})$, (47) is satisfied if $Re(c_j) = Re(\bar{c}_j) > 0$, which in turn requires:

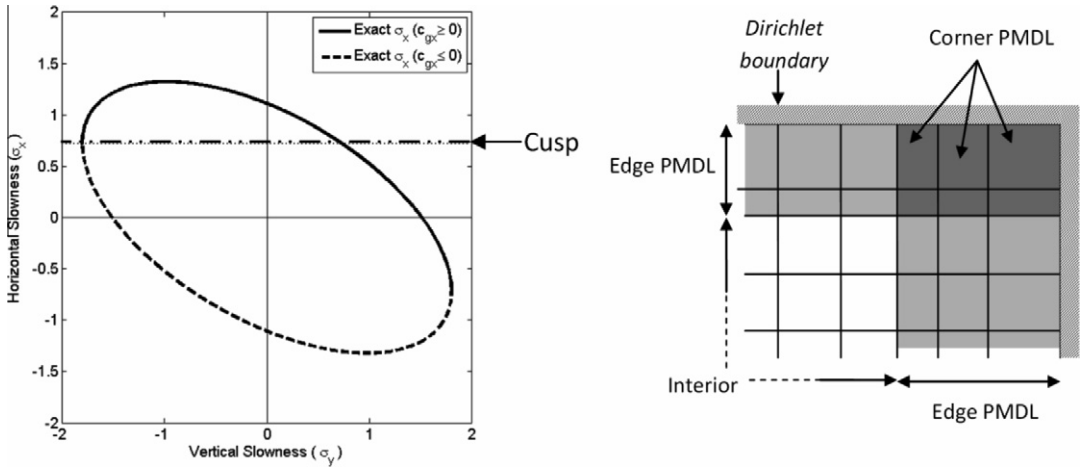

Fig. 8. *Left*: Geometric interpretation of the sufficient condition for accuracy. The parameters of PMDL should be chosen above the horizontal line that defines the 'cusp' of the ellipse. *Right*: Corner PMDL with parameters (layer lengths) consistent with the two edge PMDLs.

$$\text{for } c_j, \bar{c}_j \notin \mathbb{R}: \quad Re(c_j) = Re(\bar{c}_j) = \frac{(4AB - C^2)}{4B}\sigma_{xj} > 0 \iff \sigma_{xj} > 0. \tag{52}$$

The condition (51) encompasses (52) and (51) is hence a sufficient condition for satisfying the accuracy criterion (47). Note that (51) results in $|R_n| = 1$ for $c_{gx} = 0$; for reasons stated before, we consider this to be acceptable.

4.3. Relation between stiffness and group velocity

It should be noted that being able to express the reflection coefficient in terms of group velocities is key to the derivation of the simple accuracy condition (51). Not every ABC produces a reflection coefficient of this kind. A straightforward implementation of Higdon's multidirectional ABCs or an implementation of complex coordinate stretching in the direction of unboundedness (traditional PML) will result in a reflection coefficient of the form,

$$\widetilde{R}_n = \prod_{j=1}^{n}\left(\frac{\sigma_x - \sigma_{xj}}{\sigma_x + \sigma_{xj}}\right) = \prod_{j=1}^{n}\left(\frac{c_{pxj} - c_{px}}{c_{pxj} + c_{px}}\right), \tag{53}$$

where $c_{px_j} = 1/\sigma_{xj}$ are the reference phase velocities. For isotropic and untilted anisotropic media ($C = 0$), $c_{gx} = A/c_{px}$ from (12); approximating phase velocities is the same as approximating group velocities and a choice of $\sigma_{xj} > 0$ (or $c_{pxj} > 0$) is enough to ensure accuracy in this case. An ABC that results in a reflection coefficient of the form (53) is however not too useful for the case of tilted anisotropy because, as discussed in Section 2.4, there exist modes with positive phase velocities but with negative group velocities (and vice versa). In this case, a choice of positive reference phase velocities $c_{pxj} > 0$ is no guarantee that the ABC will accurately absorb modes with positive group velocities. While Engquist and Majda's rational approximation of the square root operator, when applied to anisotropic media, will lead to the group velocity form of the reflection coefficient (39), it is not of much practical interest because of its implementation being restricted to lower orders. Moreover, since their ABC was never developed for cases with phase and group velocities of differing signs, it is not apparent that their rational approximation was developed with the explicit goal of capturing positive group velocities.

The n-layer PMDL approximates the stiffness (18) by a rational function instead of approximating the horizontal slowness directly. It can be seen from (18) and (12) that the stiffness for propagating wave modes is in fact related to their group velocity as $K = -i\omega\, c_{gx}$. Hence, approximating stiffness is the same as approximating group velocities. It is therefore not surprising that the form of the rational approximation (25) with (21) and (22) leads us to a reflection coefficient that is expressible purely in terms of group velocities (39). As noted before, this form of (39) is *key* to the derivation of the simple accuracy condition (51).

4.4. Corners

The PMDL formulation is known to be applicable to convex polygonal corners [20,21]. Analogous to the description of corner PML in [11], a corner PMDL acts as an ABC for each of the edge PMDLs. Since the parameters of the corner PMDL are consistent with those of the edge PMDLs, as shown in Fig. 8 (right), it will absorb the corresponding 'outgoing' waves provided the parameters of *both* of the edge PMDLs satisfy (51).

5. Numerical examples

We consider a 2D model problem with a square interior consisting of a tilted anisotropic acoustic medium that is modeled by regular square bilinear finite elements. The exterior is represented by ABCs on all four edges/corners. For a given frequency ω, the characteristic wavenumber is $k = \omega/c$, with $c = \sqrt{1/a^2 + 1/b^2}$ being the velocity (see (6)). Using a conservative element size, $h = 0.05/\omega$, we get the number of elements per characteristic wavelength $N_e = 2\pi c/\omega h \approx 120$. Using the material parameters $a = 1, b = 2, \beta = 30^\circ$ in (7), the accuracy condition (51) for PMDL in the x direction is $\sigma_{xj} > 0.72$. For PMDL in the y direction we have $a = 1$, $b = 2$, $\beta = 60^\circ$ and hence (51) becomes $\sigma_{yj} > 0.98$. For simplicity, in all experiments we assume $\sigma_{yj} = 1.5\sigma_{xj}$ and $\sigma_{x1} = \sigma_{x2} = \cdots = \sigma_{xn}$, thus reducing the number the PMDL parameters to just one. The excitation consists of a normalized Gaussian given by $(\sigma\sqrt{2\pi})^{-1} e^{-(0.5(r/\sigma)^2)}$ for $r \leqslant 5\sigma$ and zero elsewhere. Here r is the radial distance from the Gaussian center and $\sigma = 1.5h$. The Gaussian center is positioned at the center of the lower left quarter. For comparison, the exact solution for tilted anisotropic medium is obtained by appropriately transforming in space, the Green's function of an isotropic medium (the Hankel function). The interior is modeled by a mesh of 600×600 finite elements with two PMDL layers forming the exterior on all four edges. The frequency is assumed to be $\omega = 1000$.

The accuracy obtained for different values of the PMDL parameters σ_{xj} can be visually inferred from Fig. 9 and is numerically quantified in Fig. 10. The relative error is calculated as $\|u_{PMDL} - u_{exact}\|_2 / \|u_{exact}\|_2$ and expressed as a percentage. The least accurate results are obtained when σ_{xj} is below the cusp i.e. when the parameters violate the accuracy criterion (51), which in the present case is $\sigma_{xj} > 0.72$. Note that we have used $\sigma_{yj} = 1.5\sigma_{xj}$ and thus the accuracy criterion is violated in the y direction too. The inaccuracies of violating (51) are dramatic in the first two snapshots of Fig. 9.

Fig. 10 shows that the minimum relative error obtained with a 2-layer PMDL is around 1%. It should be noted that this includes the interior discretization error which can be reduced with a reduction in the interior element size; experiments with finer interior discretizations have confirmed this. Since we wish to compare the relative effect of changing PMDL parameters, our observations are valid as long as the interior discretization remains constant.

The relative error is also seen to increase when the parameters are chosen above the peak of the ellipse. This is because of the fact that for such parameters there will be no interpolation points on the ellipse and since we wish to capture a part of

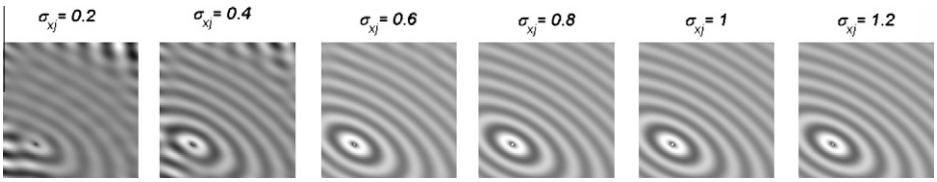

Fig. 9. Interior solution for a 2 layer PMDL exterior with various PMDL parameters. The first three have parameters under the cusp and thus violate the accuracy criterion.

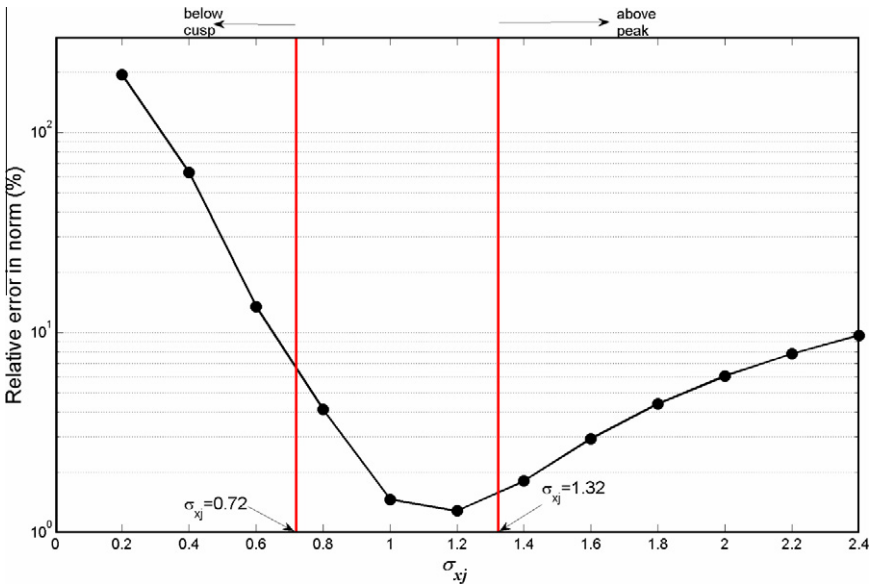

Fig. 10. Relative error in norm for a 2 layer PMDL with various parameters. The lines demarcating the cusp of the slowness ellipse and its peak are shown.

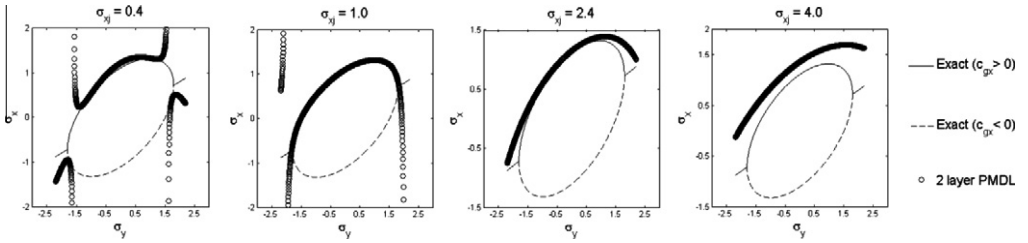

Fig. 11. Slowness diagrams for 2 layer PMDL approximation with parameters chosen below the cusp, between the cusp and peak and above the peak.

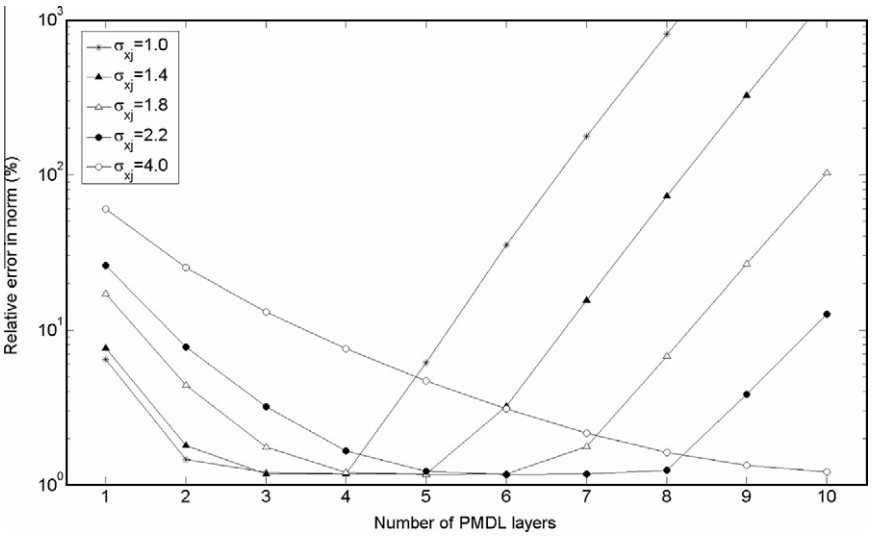

Fig. 12. Relative error in PMDL approximation with increasing number of PMDL layers for various PMDL parameters that satisfy the accuracy criterion.

the ellipse (the positive group velocity part) we should expect some loss in accuracy in this case. The slowness diagrams presented in Fig. 11 clearly demonstrate this. The case of $\sigma_{xj} = 0.4$ violates (51) with the parameter being below the cusp and the capturing of the negative group velocity branch is evident. The remaining three cases with $\sigma_{xj} = 1.0, 2.4, 4.0$ all lie above the cusp and hence approximate the positive group velocity branch only. However $\sigma_{xj} = 1.0$ also lies under the peak and hence interpolates the ellipse at $\sigma_x = 1.0$. The last two cases lie beyond the peak and hence have no points of interpolation with the exact curve.

It is expected that increasing the number of PMDL layers should reduce the error in approximation as long as (51) is satisfied. The relative error in approximation with increasing number of PMDL layers for various PMDL parameters that satisfy (51) is shown in Fig. 12 and it depicts a clear worsening of the approximation with increasing number of PMDL layers especially for lower PMDL parameters. This counter intuitive behavior can be explained by studying the slowness diagrams shown in Fig. 13 for a large number of PMDL layers. Since the parameters of PMDL were chosen to be real, they approximate the propagating part of the slowness curve (the tilted ellipse) without capturing the evanescent part (σ_y beyond the ellipse). As the number of layers increase, the PMDL approximates the propagating part of the slowness curve with rational polynomials of increasing degrees. While this results in a better approximation inside the ellipse, just outside the ellipse, however,

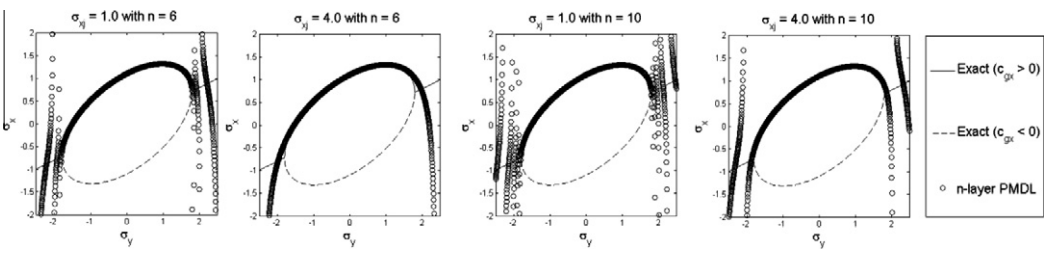

Fig. 13. Slowness diagrams for large number of PMDL layers (6) and (10) with different PMDL parameters.

it invariably leads to the very highly oscillatory behavior typical of high degree rational functions due to the increasing number of alternating poles and zeros. This indicates that there are large errors in the evanescent spectrum, leading to worsening of the solution quantified in Fig. 12. The interior solution corresponding to the slowness diagrams of Fig. 13 are shown in Fig. 14 and clearly show the desired solution being polluted near the boundary ($\sigma_{xj} = 1.0, n = 6$) and being completely overshadowed throughout the interior ($\sigma_{xj} = 1.0, n = 10$).

Notice however, that using parameters far above the cusp, $\sigma_{xj} = 4.0 \gg 0.72$ for instance, will result in a bad approximation for smaller number of layers, but a much better approximation for larger number of layers according to Fig. 12. This can be explained by comparing the last diagram in Fig. 11 ($\sigma_{xj} = 4.0, n = 2$) with the second and fourth diagrams in Fig. 13 ($\sigma_{xj} = 4.0, n = 6, 10$). It is also interesting to note that the error does not reduce beyond 1% (approximately) irrespective of the number of PMDL layers used with any parameter satisfying the accuracy criterion (51). With the knowledge that this minimum error reduces with finer interior discretization (not shown here), we can conclude that (a) this 1% error is mainly due to the interior discretization and (b) just 2–3 PMDL layers are sufficient to reduce the error to the interior discretization error as long as the parameters of PMDL satisfy the accuracy criterion.

We conclude this section with two methods for handling the errors due to the presence of clustered zeros and poles for large number of PMDL layers. Just like PMDL layers with real parameters capture propagating waves, PMDL layers with *imaginary* or *complex* parameters have been shown to capture decaying waves (with purely imaginary and complex wavenumbers) [22,38]. These are termed the *padding* layers (purely imaginary parameters) and *complex PMDL* (complex parameters). The performance of PMDL with varying number of padding layers is shown in Fig. 15. The parameters of the padding layers are chosen as those that smoothen the highly oscillatory part of the slowness curves the most. Similar results are obtained for PMDL parameters chosen much above the cusp $\sigma_{xj} \gg 0.72$. The slowness diagrams with padding and complex layers and their visual snapshots are shown in Fig. 16, 17, and 18. The smoothening of the real part of the slowness approximation is evident in Fig. 16; this leads to a better approximation of propagating waves. The imaginary part of the approximation is shown in Fig. 17; the presence of the non-zero imaginary part in the approximation models decaying waves appropriately. The corresponding snapshots can be seen in Fig. 18.

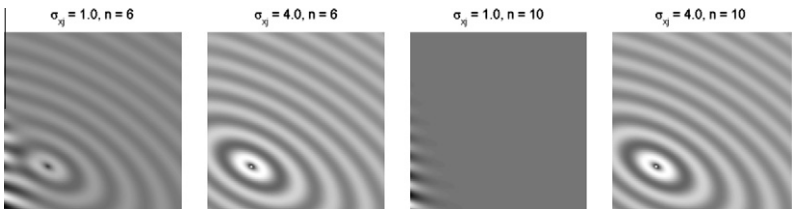

Fig. 14. Interior solution for large number of PMDL layers ($n = 6, 10$) with PMDL parameters chosen above and near the cusp ($\sigma_{xj} = 1.0$) and above and far away from the cusp ($\sigma_{xj} = 4.0$).

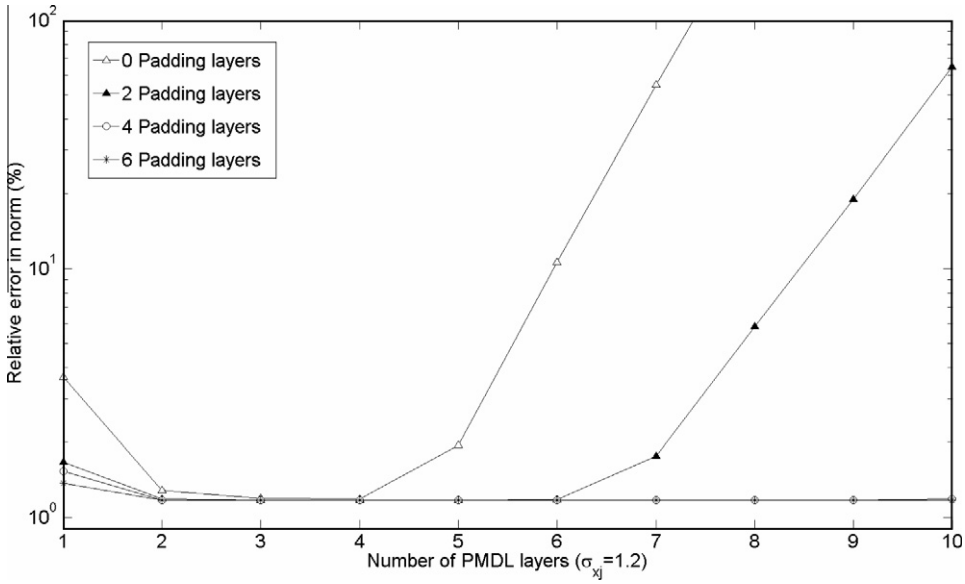

Fig. 15. Performance of PMDL when used along with padding layers.

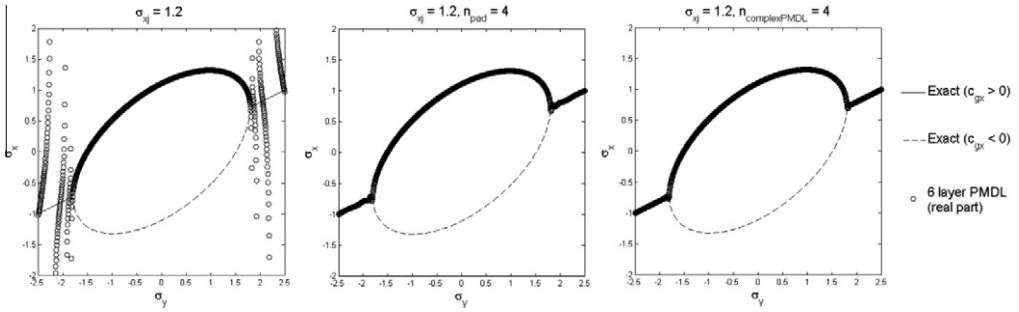

Fig. 16. Real part of the slowness approximation for 6 layer PMDL with $\sigma_{xj} = 1.2$ and with padding layers and complex PMDL layers.

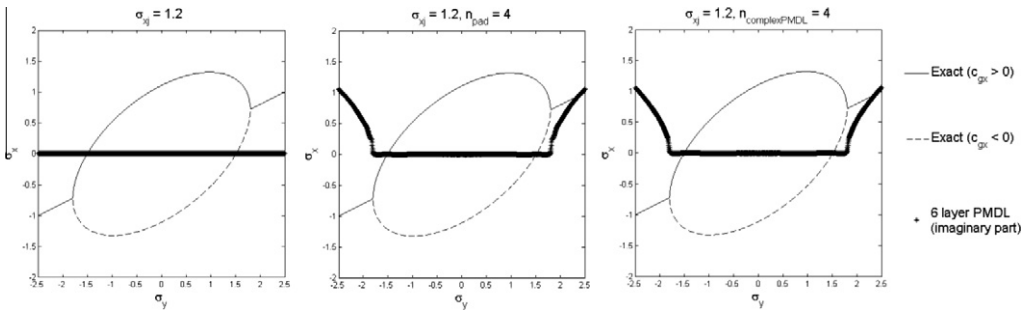

Fig. 17. Imaginary part of the slowness approximation for 6 layer PMDL with $\sigma_{xj} = 1.2$ and with padding layers and complex PMDL layers.

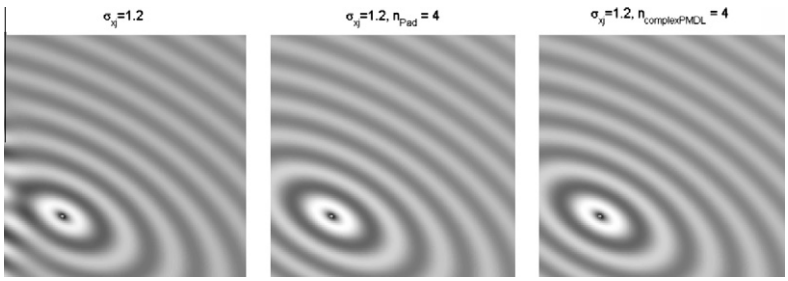

Fig. 18. Interior solution for 6 layer PMDL with $\sigma_{xj} = 1.2$ and with padding layers and complex PMDL layers.

6. Summary and Conclusions

A sufficient condition for the accuracy of PMDL ABC for the time harmonic modeling of scalar waves in an anisotropic acoustic medium is presented. In deriving this accuracy criterion, the PMDL formulation is shown to naturally overcome challenges posed by the existence of wave modes with differing phase and group velocity signs *without the need of an explicit coordinate transformation;* the absence of such transformations make the current study more amenable to extensions involving layered media. The distinctive property of PMDL, namely approximation of half-space stiffness instead of the wavenumber, is central to the ability of PMDL to capture the correct group velocities even when the group and phase velocities are not aligned in the same direction. This is because the group velocity and stiffness are related (at least in this case) and PMDL approximates the stiffness. We hypothesize that the link between group velocity and stiffness extends to general vector systems and that this link can be used to ensure accuracy of PMDL in general anisotropic media.

PMDL is known to possess several advantages over other local ABCs and is thus used for the present study. The PMDL derivation is applicable to any second order hyperbolic system and to general anisotropic, heterogeneous exteriors, with heterogeneity confined to directions orthogonal to the direction of unboundedness. PMDL is equally applicable to propagating and evanescent waves and can be implemented to an arbitrarily high degree of accuracy without discretization errors. PMDL is also linked to PML and show promise in inheriting their versatility.

The present study is confined to propagating scalar wave modes in homogeneous (though anisotropic) exteriors. Since none of these restrictions are due to actual limitations of the PMDL formulation, further studies will (hopefully) eliminate

all of them. Establishing links between group velocity and stiffness for complicated media and taking evanescent waves into account are of immediate concern. Further developments need to address more complex vector wave equations related to anisotropic electromagnetism and elastodynamics.

References

[1] D. Givoli, Nonreflecting boundary-conditions, J. Comput. Phys. 1 (1991) 1–29.
[2] S.V. Tsynkov, Numerical solution of problems on unbounded domains: A review, Appl. Numer. Math. 4 (1998) 465–532.
[3] T. Hagstrom, New results on absorbing layers and radiation boundary conditions, Topics in Computational Wave Propagation – Direct and Inverse Problems (2003) 1–42.
[4] E.L. Lindman, Free-space boundary-conditions for time-dependent wave-equation, J. Comput. Phys. 1 (1975) 66–78.
[5] B. Engquist, A. Majda, Absorbing boundary-conditions for numerical-simulation of waves, Math. Comput. 139 (1977) 629–651.
[6] B. Engquist, A. Majda, Radiation boundary-conditions for acoustic and elastic wave calculations, Commun. Pure Appl. Math. 3 (1979) 313–357.
[7] A. Bayliss, E. Turkel, Radiation boundary-conditions for wave-like equations, Commun. Pure Appl. Math. 6 (1980) 707–725.
[8] R.L. Higdon, Numerical absorbing boundary-conditions for the wave-equation, Math. Comput. 179 (1987) 65–90.
[9] D. Givoli, High-order local non-reflecting boundary conditions: a review, Wave Motion 4 (2004) 319–326.
[10] T. Hagstrom, A. Mar-Or, D. Givoli, High-order local absorbing conditions for the wave equation: extensions and improvements, J. Comput. Phys. 6 (2008) 3322–3357.
[11] J.P. Bérenger, A perfectly matched layer for the absorption of electromagnetic-waves, J. Comput. Phys. 2 (1994) 185–200.
[12] W.C. Chew, J.M. Jin, E. Michielssen, Complex coordinate stretching as a generalized absorbing boundary condition, Microwave Opt. Technol. Lett. 6 (1997) 363–369.
[13] W.C. Chew, W.H. Weedon, A 3D perfectly matched medium from modified Maxwells equations with stretched coordinates, Microwave Opt. Technol. Lett. 13 (1994) 599–604.
[14] Z.S. Sacks, D.M. Kingsland, R. Lee, J.F. Lee, A perfectly matched anisotropic absorber for use as an absorbing boundary condition, IEEE Trans. Antennas Propag. 12 (1995) 1460–1463.
[15] F.L. Teixeira, W.C. Chew, Analytical derivation of a conformal perfectly matched absorber for electromagnetic waves, Microwave Opt. Technol. Lett. 17 (1998) 231–236.
[16] Kuzuoglu, Mittra, Frequency dependence of the constitutive parameters of causal perfectly matched anisotropic absorbers, IEEE Microwave Guided Wave Lett. 12 (1996) 447.
[17] Roden, Gedney, Convolution PML (CPML): an efficient FDTD implementation of the CFS-PML for arbitrary media, Microwave Opt. Technol. Lett. 5 (2000) 334.
[18] Meza-Fajardo, Papageorgiou, A nonconvolutional, split-field, perfectly matched layer for wave propagation in isotropic and anisotropic elastic media: stability analysis, Bull. Seismological Soc. Am. 4 (2008) 1811–1836.
[19] S. Asvadurov, V. Druskin, M.N. Guddati, L. Knizhnerman, On optimal finite-difference approximation of PML, SIAM J. Numer. Anal. 1 (2003) 287–305.
[20] K.W. Lim, Absorbing boundary conditions for corner regions, Master's Thesis, North Carolina State University, 2003.
[21] M.N. Guddati, K.W. Lim, Continued fraction absorbing boundary conditions for convex polygonal domains, Int. J. Numer. Methods Eng. 6 (2006) 949–977.
[22] M.N. Guddati, K.W. Lim, M.A. Zahid, Perfectly matched discrete layers for unbounded domain modeling, in: F. Magoulès (Ed.), Computational Methods for Acoustics Problem, Saxe-Coburg Publications, Scotland, 2008, pp. 69–98.
[23] C.K.W. Tam, L. Auriault, F. Cambuli, Perfectly matched layer as an absorbing boundary condition for the linearized Euler equations in open and ducted domains, J. Comput. Phys. 144 (1998) 213–234.
[24] E. Turkel, A. Yefet, Absorbing PML boundary layers for wave-like equations, Appl. Numer. Math. 27 (1998) 533–557.
[25] S. Abarbanel, D. Gottlieb, J.S. Hesthaven, Well-posed perfectly matched layers for advective acoustics, J. Comput. Phys. 2 (1999) 266–283.
[26] F.Q. Hu, A stable perfectly matched layer for linearized Euler equations in unsplit physical variables, J. Comput. Phys. 2 (2001) 455–480.
[27] T. Hagstrom, A new construction of perfectly matched layers for hyperbolic systems with applications to the linearized Euler equations, in: Cohen et al. (Ed.), Mathematical and Numerical Aspects of Wave Propagation, Proceedings Waves 2003, Springer-Verlag, 2003, pp. 125–129.
[28] E. Bécache, S. Fauqueux, P. Joly, Stability of perfectly matched layers, group velocities and anisotropic waves, J. Comput. Phys. 2 (2003) 399–433.
[29] E. Bécache, A.S. Bonnet-Ben Dhia, G. Legendre, Perfectly matched layers for the convected Helmholtz equation, SIAM J. Numer. Anal. 1 (2004) 409–433.
[30] F.Q. Hu, A perfectly matched layer absorbing boundary condition for linearized Euler equations with a non-uniform mean flow, J. Comput. Phys. 208 (2005) 469–492.
[31] E. Bécache, A.S.B.B. Dhia, G. Legendre, Perfectly matched layers for time-harmonic acoustics in the presence of a uniform flow, SIAM J. Numer. Anal. 3 (2006) 1191–1217.
[32] J. Diaz, P. Joly, A time domain analysis of PML models in acoustics, Comput. Methods Appl. Mech. Eng. 29–32 (2006) 3820–3853.
[33] S. Parrish, F. Hu, PML absorbing boundary conditions for the linearized and nonlinear Euler equations in the case of oblique mean flow, Int. J. Numer. Methods Fluids 60 (2009) 565–589.
[34] E. Becache, D. Givoli, T. Hagstrom, High-order absorbing boundary conditions for anisotropic and convective wave equations, J. Comput. Phys. 229 (2010) 1099–1129.
[36] S. Savadatti, M.N. Guddati, Absorbing boundary conditions for scalar waves in anisotropic media. Part 2: Time-dependent modeling, J. Comput. Phys. 228 (2010) 6644–6662.
[37] M.N. Guddati, J.L. Tassoulas, Continued-fraction absorbing boundary conditions for the wave equation, J. Comput. Acoust. 1 (2000) 139–156.
[38] M.N. Guddati, Arbitrarily wide-angle wave equations for complex media, Comput. Methods Appl. Mech. Eng. 1–3 (2006) 65–93.
[39] T. Hagstrom, T. Warburton, A new auxiliary variable formulation of high-order local radiation boundary conditions: corner compatibility conditions and extensions to first-order systems, Wave Motion 4 (2004) 327–338.
[40] T. Hagstrom, T. Warburton, Complete radiation boundary conditions: minimizing the long time error growth of local methods, <http://faculty.smu.edu/thagstrom/HWcomplete.pdf>, 2008.
[41] R.L. Higdon, Initial-boundary value-problems for linear hyperbolic systems, SIAM Rev. 2 (1986) 177–217.